Negative differential thermal conductance through vacuum

Linxiao Zhu,[1] Clayton R. Otey,[1] and Shanhui Fan[2,a)]
[1]*Department of Applied Physics, Stanford University, Stanford, California 94305, USA*
[2]*Department of Electrical Engineering, Ginzton Laboratory, Stanford University, Stanford, California 94305, USA*

(Received 6 September 2011; accepted 8 January 2012; published online 26 January 2012)

We propose a scheme for achieving negative differential thermal conductance in near-field electromagnetic thermal transfer. As an example, we show that the scheme can be implemented with two slabs of silicon carbide brought in close proximity to each other. We also describe how a bistable thermal switch can be constructed in this manner. © *2012 American Institute of Physics*. [doi:10.1063/1.3679694]

Consider two thermal bodies 1 and 2, at temperatures T_1 and T_2, with $T_1 > T_2$. Bringing them into thermal contact will result in a heat flux per area Q that flows from body 1 to 2. For this system, we define the differential thermal conductances $(\partial Q/\partial T_1)|_{T_2}$ and $(-\partial Q/\partial T_2)|_{T_1}$. Typically, these conductances are both positive, since the heat flux typically increases with the increase of the temperature difference. When the opposite is true, i.e., when either $(\partial Q/\partial T_1)|_{T_2}$ or $(-\partial Q/\partial T_2)|_{T_1}$ becomes negative, the system exhibits a negative differential thermal conductance.

Negative differential thermal conductance is a direct thermal analogue of the negative differential electrical conductance, an effect that has been widely exploited in electronic circuit design.[1–3] The phenomenon of negative differential thermal conductance[4] has attracted recent interest as a key building block of thermal circuits.[5] Reference 4 uses phonon as thermal carrier. In contrast, here, we theoretically demonstrate that negative differential thermal conductance can be observed using photon as the thermal carrier.

To study photon-based thermal transport, we consider thermal bodies separated by vacuum as shown in Fig. 1(a). If these bodies were blackbodies, and we assume that they each have an *infinite* flat surface facing each other, applying Stefan's law, heat flux density (i.e., heat flux per unit area) from body 1 to 2 is $Q = \sigma(T_1^4 - T_2^4)$, where σ is the Stefan-Boltzmann constant. Thus, differential thermal conductances $(\partial Q/\partial T_1)|_{T_2}$ and $(-\partial Q/\partial T_2)|_{T_1}$ are both positive.

To achieve negative differential thermal conductance for photonic system, we build upon and extend concepts that has been proposed to achieve photonic thermal rectification.[6,7] Instead of using blackbodies that have very broadband thermal electromagnetic fields, we assume that both bodies support narrow-band resonances in its thermal electromagnetic fields. Here, again, we assume that these bodies both have flat infinite surfaces facing each other. Thus, significant thermal transfer occurs only when the resonances overlap. We further assume that the frequencies of these resonances are temperature dependent.

Suppose we have two bodies made of the same material, the resonance frequencies of the two bodies should then align when $T_1 = T_2$, as shown in Fig. 1(b). If we increase the temperature bias, by either increasing the temperature T_1 of body 1 or by decreasing the temperature T_2 of body 2, the resonances of the two bodies will start to misalign, as shown in Fig. 1(c). Such a misalignment may lead to the reduction of thermal transfer, and hence the possibility of negative differential thermal conductance, at sufficiently large temperature difference between the two bodies.

As a concrete implementation, we consider the system shown in the inset of Fig. 2(b), where two bodies of SiC of the 6H polytype are placed in close proximity to each other. The extraordinary axis is set normal to the slab surfaces. SiC-vacuum interface supports well defined surface phonon-polariton which dominates the thermal electromagnetic fields in the near field.[8–12] The temperature dependence of the optical phonon frequencies for bulk SiC was provided in Refs. 10 and 12. The temperature dependence of the surface phonon-polariton frequency at the SiC-vacuum interface can be directly calculated from these data. The calculated resonance frequency is temperature dependent as depicted in Figs. 1(b) and 1(c), satisfying the operating principles as outlined above.

To calculate the heat flux for this system, we follow closely the computational procedure described in details in Refs. 6, 13 and 14. Very briefly, we use Rytov's formalism where thermal transport is modeled by considering fluctuating current sources in each body, with the amplitude of the fluctuation related to both the temperature of the body and the imaginary part of the dielectric constant. The heat flux is then determined by integrating the contributions from all sources. The result of the calculation is the spectral heat flux per area from body 1 to body 2

$$S(\omega) = [\Theta(\omega, T_1) - \Theta(\omega, T_2)] \int d\vec{\beta} \frac{2}{\pi^3} |k_{zv}|^2 \times \left[\frac{Re(k_{z1o}) Re(k_{z2o})}{|C_\perp|^2} + \frac{Re(\epsilon_{1o}^* k_{z1e}) Re(\epsilon_{2o}^* k_{z2e})}{|C_P|^2} \right]. \quad (1)$$

The integration of $S(\omega)$ over ω results in heat flux per area Q from body 1 to body 2. In Eq. (1), $\Theta(\omega, T) = \frac{\hbar\omega}{e^{\hbar\omega/k_B T} - 1}$ is the mean thermal energy for a given mode at a frequency ω,

a)Author to whom correspondence should be addressed. Electronic mail: shanhui.fan@stanford.edu.

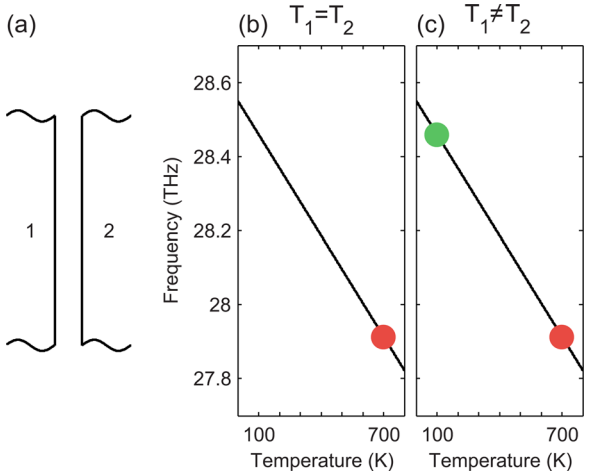

FIG. 1. (Color online) (a) The schematic of a system made of body 1 and body 2. (b) and (c) Two bodies are made of the same material and the black lines denote the temperature dependence of electromagnetic resonance of such material. (b) illustrates the case of $T_1 = T_2$ and (c) illustrates the case of $T_1 \neq T_2$. For concreteness, the curve shown here is the surface phonon-polariton frequency of silicon carbide of the 6H polytype, with the extraordinary axis normal to the surface.

$$
\begin{aligned}
k_{z1o} &= \sqrt{\epsilon_{1o}(\omega/c)^2 - \beta^2}, \quad k_{z2o} = \sqrt{\epsilon_{2o}(\omega/c)^2 - \beta^2} \\
k_{zv} &= \sqrt{(\omega/c)^2 - \beta^2}, \quad k_{z1e} = \sqrt{\epsilon_{1o}(\omega/c)^2 - \beta^2 \epsilon_{1o}/\epsilon_{1e}} \\
k_{z2e} &= \sqrt{\epsilon_{2o}(\omega/c)^2 - \beta^2 \epsilon_{2o}/\epsilon_{2e}} \\
C_P &= (\epsilon_{1o}k_{zv} + k_{z1e})(\epsilon_{2o}k_{zv} + k_{z2e})e^{ik_{zv}d} \\
&\quad -(\epsilon_{1o}k_{zv} - k_{z1e})(\epsilon_{2o}k_{zv} - k_{z2e})e^{-ik_{zv}d} \\
C_\perp &= (k_{zv} + k_{z1o})(k_{zv} + k_{z2o})e^{ik_{zv}d} \\
&\quad -(k_{zv} - k_{z1o})(k_{zv} - k_{z2o})e^{-ik_{zv}d}.
\end{aligned}
\tag{2}
$$

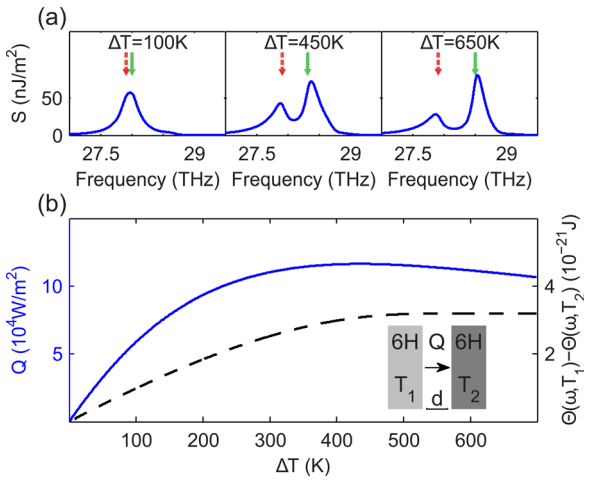

FIG. 2. (Color online) (a) Spectral heat flux between body 1 and body 2 at different $\Delta T \equiv T_1 - T_2$, for the device made of two SiC-6H slabs as shown in the inset of (b), with $T_1 = 700\ K$ and separation $d = 100$ nm. In each subplot, the red dashed arrow and green solid arrow denote the surface phonon-polariton frequencies for body 1 and body 2, respectively, as shown in Figs. 1(b) and 1(c). (b) The blue solid line, pertaining to the left y axis, is the net heat flux between body 1 and body 2 as a function of ΔT for the device shown in the inset, with $T_1 = 700$ K and $d = 100$ nm. The black dashed line, pertaining to the right y axis, shows $[\Theta(\omega,T_1) - \Theta\ (\omega,T_2)]$ as a function of ΔT, with $T_1 = 700$ K and ω corresponding to the surface phonon-polariton frequency of 6H silicon carbide at 700 K (Figs. 1(b) and 1(c)).

Here, ϵ's are the dielectric constants, β is transverse wavenumber, and the o and e subscripts correspond to the ordinary and the extraordinary axes, respectively.

As shown in Eq. (1), $S(\omega)$ contains a factor $[\Theta(\omega,T_1) - \Theta\ (\omega,T_2)]$, which increases monotonously as $\Delta T \equiv T_1 - T_2$ increases. The remaining part in $S(\omega)$ has an implicit dependence on temperature since the dielectric constants of the materials change with temperature.

Using Eq. (1), we study the thermal transfer properties of a few structures. We first set the spacing of the bodies at $d = 100$ nm and $T_1 = 700$ K. We vary T_2 while maintaining $T_1 > T_2$. We plot the net heat flux between the bodies as a function of temperature bias $\Delta T \equiv T_1 - T_2$ in Fig. 2(b) (blue solid line). At small ΔT, the heat flux increases as ΔT. The heat flux reaches a maximum at $\Delta T = 435\ K$, beyond which the heat flux starts to decrease as a function of ΔT. The system thus exhibits the effect of negative differential thermal conductance.

Below, we illustrate the physical mechanism of negative differential thermal conductance, by considering the thermal electromagnetic field spectra at various temperature biases (Fig. 2(a)). Since the system is in the near-field regime, with the separation d far below the thermal wavelengths, the spectra consist of resonant peaks. The location of the peaks is well aligned with the surface phonon-polariton frequencies of the two SiC-vacuum interfaces. In Fig. 2(a), we keep the temperature of body 1 fixed. We see that, for all temperature biases, there is always a peak in the vicinity of 27.91 THz (red dashed arrow, Fig. 2(a)). The location of this peak corresponds very well to the frequency of surface phonon-polariton at the interface between vacuum and body 1. On the other hand, we see a second spectral peak (green solid arrow, Fig. 2(a)) moving towards higher frequency, as we increase the temperature bias and hence decrease T_2. This second peak corresponds to the surface phonon-polariton at the interface between vacuum and body 2. Combining Figs. 2(a) and 2(b), we can, therefore, attribute the existence of negative differential thermal transfer, to the temperature dependence of the surface phonon-polariton frequencies at the two interfaces.

In Fig. 2, we have demonstrated negative differential thermal conductance, in a scenario where the temperature gradient is increased through the decrease of temperature T_2 of the colder body. In such a scenario, the difference in mean thermal energy per mode, i.e., $[\Theta(\omega,T_1) - \Theta\ (\omega,T_2)]$, varies relatively slowly as a function of T_2 and, in fact, saturates when T_2 is sufficiently low (dashed curve, Fig. 2(b)). Hence, the behavior of the spectral thermal flux $S(\omega)$ is largely determined by the temperature dependence of the dielectric constant. For this scenario, our proposed mechanism through a temperature-dependent spectral misalignment is very effective.

In contrast to the scenario above, we now consider in Fig. 3 an alternative scenario, where we instead increase the temperature differences between the bodies through an increase of the temperature T_1 of the hotter body, while keeping the temperature T_2 of the colder body fixed. In this case, the difference in mean thermal energy per mode, i.e., $[\Theta(\omega,T_1) - \Theta\ (\omega,T_2)]$, increases drastically as T_1 increases, making it more difficult to achieve negative differential

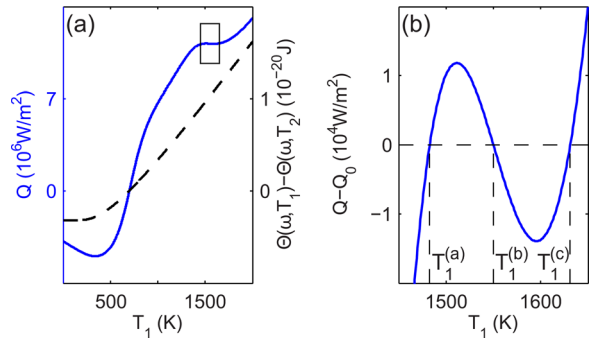

FIG. 3. (Color online) (a) The blue solid line is the net heat flux between body 1 and body 2 as a function of T_1, for the device made of two SiC-6H slabs as shown in the inset of Fig. 2(b), with $T_2 = 700$ K and $d = 10$ nm. The black dashed line shows $[\Theta(\omega,T_1) - \Theta(\omega,T_2)]$ as a function of T_1, with $T_2 = 700$ K and ω corresponding to the surface phonon-polariton frequency of 6H silicon carbide at 700 K (Figs. 1(b) and 1(c)). (b) Operating region of a bi-stable thermal switch, corresponding to the rectangle in (a). Q_0 is a constant external heat flux into body 1. Here, we assume that $Q_0 = 1.1185 \times 10^7$ W/m^2.

thermal conductance (dashed curve, Fig. 3(a)). In Fig. 3, we see that negative differential conductance is nevertheless accomplished, but at a much closer spacing $d = 10$ nm between the two bodies, and with a much larger temperature difference.

An interesting implication of negative differential thermal conductance is the effect of thermal bistability. As an illustration, we again consider the system shown in Fig. 3, where we provide, in Fig. 3(b), an enlarged view of the region exhibiting negative differential thermal conductance. In this region, in equilibrium, at a constant externally injected heat flux Q_0 through the system (dashed line, Fig. 3(b)), with T_2 fixed, body 1 can exhibit three different equilibrium temperatures $T_1^{(a)} < T_1^{(b)} < T_1^{(c)}$. These different temperatures have different stability: Denoting any of these temperatures $T_1^{(0)}$, and assuming a small temperature fluctuation δT of body 1 around $T_1^{(0)}$, we then have

$$C\frac{d(\delta T)}{dt} = Q_0 - Q(T) = Q_0 - Q(T_1^{(0)}) + Q(T_1^{(0)}) - Q(T)$$

$$= -\left.\frac{dQ}{dT}\right|_{T_1^{(0)}} \delta T,$$

where C is the heat capacity of body 1. We see, therefore, that a negative dQ/dT implies an instability with respect to temperature fluctuation. Thus, only $T_1^{(a)}$and $T_1^{(c)}$in Fig. 3(b) correspond to a stable situation. With a constant externally injected heat flux, the system, therefore, is a bi-stable thermal switch.

As final remarks, we comment on some of the considerations for the experimental realization of our prediction. The slab-to-slab separation that we assume, at a distance of 10–100 nm, should be technically feasible in light of recent thermal transfer experiments.[9,15,16] Our theory is directly applicable to planar structures, with relatively large surface areas. Very recently, enhanced near-field thermal transfer has been observed in Ref. 16, which uses a structure with a surface area of a few mm^2. The excellent agreement between theory and experiment in Ref. 16 indicates that at such a surface area, finite-size effect is not important. This is the same regime that we are predicting our effects as well. To demonstrate our effect, the bodies need to be maintained at a constant temperature, hence the bodies need to be efficiently connected to a heat sink. The typical amount of heat flow for the structure in Fig. 2(b) is approximately 110 000 W/m^2. In Refs. 9 and 15, one can infer a maximum heat flux of about 62 000 W/m^2 for a small area device. Our heat flow density is comparable. We have a much larger area, thus the need to maintain constant temperature at the surface should be less severe. The thermal expansion of SiC can cause gap size to change by as much as a few nm. However, all the near field experiments use feedback control scheme to maintain a constant gap size. Finally, while for simplicity, we have used a planar geometry, we expect similar effects might be observed in other experimental geometries as well, provided the bodies support tunable, temperature dependent electromagnetic resonances.

This work is supported by an AFOSR-MURI program (Grant No. FA9550-08-1-0407) and by the Division of Materials Sciences and Engineering, Office of Basic Energy Sciences, the U. S. Department of Energy.

[1]L. Esaki and R. Tsu, IBM J. Res. Dev. **14**, 61 (1970).
[2]A. Seabaugh, Y.-C. Kao, and H.-T. Yuan, IEEE Electron Device Lett. **13**, 479 (1992).
[3]T. Broekaert, B. Brar, J. van der Wagt, A. Seabaugh, F. Morris, T. Moise, E. Beam, and G. Frazier, IEEE J. Solid-State Circuits **33**, 1342 (1998).
[4]B. Li, L. Wang, and G. Casati, Appl. Phys. Lett. **88**, 143501 (2006).
[5]L. Wang and B. Li, Phys. World **21**, 27 (2008).
[6]C. R. Otey, W. T. Lau, and S. Fan, Phys. Rev. Lett. **104**, 154301 (2010).
[7]S. Basu and M. Francoeur, Appl. Phys. Lett. **98**, 113106 (2011).
[8]A. V. Shchegrov, K. Joulain, R. Carminati, and J.-J. Greffet, Phys. Rev. Lett. **85**, 1548 (2000).
[9]E. Rousseau, A. Siria, G. Jourdan, S. Volz, F. Comin, J. Chevrier, and J.-J. Greffet, Nature Photon. **3**, 514 (2009).
[10]W. G. Spitzer, D. Kleinman, and D. Walsh, Phys. Rev. **113**, 127 (1959).
[11]W. G. Spitzer, D. A. Kleinman, and C. J. Frosch, Phys. Rev. **113**, 133 (1959).
[12]D. Olego and M. Cardona, Phys. Rev. B **25**, 3889 (1982).
[13]D. Polder and M. Van Hove, Phys. Rev. B **4**, 3303 (1971).
[14]J. J. Loomis and H. J. Maris, Phys. Rev. B **50**, 18517 (1994).
[15]S. Shen, A. Narayanaswamy, and G. Chen, Nano Lett. **9**, 2909 (2009).
[16]R. S. Ottens, V. Quetschke, S. Wise, A. A. Alemi, R. Lundock, G. Mueller, D. H. Reitze, D. B. Tanner, and B. F. Whiting, Phys. Rev. Lett. **107**, 014301 (2011).